OPEN ACCESS



A Uniform Type Ia Supernova Distance Ladder with the Zwicky Transient Facility: Absolute Calibration Based on the Tip of the Red Giant Branch Method

Suhail Dhawan¹, Ariel Goobar², Joel Johansson², In Sung Jang³, Mickael Rigault⁴, Luke Harvey⁵, Kate Maguire⁵, Wendy L. Freedman³, Barry F. Madore⁶, Mathew Smith⁴, Jesper Sollerman⁷, Young-Lo Kim⁸, Igor Andreoni⁹, Eric C. Bellm¹⁰, Michael W. Coughlin¹¹, Richard Dekany¹², Matthew J. Graham¹³, Shrinivas R. Kulkarni¹³, Russ R. Laher¹⁴, Michael S. Medford^{15,16}, James D. Neill¹³, Guy Nir¹⁷, Reed Riddle¹², and Ben Rusholme¹⁴ Institute of Astronomy and Kavli Institute for Cosmology, University of Cambridge, Madingley Road, Cambridge CB3 0HA, UK; suhail.dhawan@ast.cam.ac.uk The Oskar Klein Centre for Cosmoparticle Physics, Department of Physics, Stockholm University, SE-10691 Stockholm, Sweden ³ Department of Astronomy & Astrophysics & Kavli Institute for Cosmological Physics, University of Chicago, 5640 South Ellis Avenue, Chicago, IL 60637, USA Univ Lyon, Univ Claude Bernard Lyon 1, CNRS/IN2P3, IP2I Lyon, UMR 5822, F-69622, Villeurbanne, France School of Physics, Trinity College Dublin, The University of Dublin, Dublin 2, Ireland ⁶ The Observatories of the Carnegie Institution for Science, 813 Santa Barbara St., Pasadena, CA 91101, USA The Oskar Klein Centre, Department of Astronomy, Stockholm University, SE-10691 Stockholm, Sweden Department of Physics, Lancaster University, Lancashire LA1 4YB, UK ⁹ Department of Astronomy, University of Maryland, College Park, MD 20742, USA ¹⁰ DIRAC Institute, Department of Astronomy, University of Washington, 3910 15th Avenue NE, Seattle, WA 98195, USA School of Physics and Astronomy, University of Minnesota, Minneapolis, Minnesota 55455, USA Caltech Optical Observatories, California Institute of Technology, Pasadena, CA 91125, USA ¹³ Division of Physics, Mathematics, and Astronomy, California Institute of Technology, Pasadena, USA IPAC, California Institute of Technology, 1200 E. California Blvd, Pasadena, CA 91125, USA University of California, Berkeley, Department of Astronomy, Berkeley, CA 94720, USA Lawrence Berkeley National Laboratory, 1 Cyclotron Rd., Berkeley, CA 94720, USA ¹⁷ Department of Astronomy, University of California, Berkeley, CA 94720-3411, USA Received 2022 March 8; revised 2022 June 27; accepted 2022 June 27; published 2022 August 5

Abstract

The current Cepheid-calibrated distance ladder measurement of H_0 is reported to be in tension with the values inferred from the cosmic microwave background (CMB), assuming standard cosmology. However, some tip of the red giant branch (TRGB) estimates report H_0 in better agreement with the CMB. Hence, it is critical to reduce systematic uncertainties in local measurements to understand the Hubble tension. In this paper, we propose a uniform distance ladder between the second and third rungs, combining Type Ia supernovae (SNe Ia) observed by the Zwicky Transient Facility (ZTF) with a TRGB calibration of their absolute luminosity. A large, volume-limited sample of both calibrator and Hubble flow SNe Ia from the *same* survey minimizes two of the largest sources of systematics: host-galaxy bias and nonuniform photometric calibration. We present results from a pilot study using the existing TRGB distance to the host galaxy of ZTF SN Ia SN 2021rhu (aka ZTF21abiuvdk) in NGC7814. Combining the ZTF calibrator with a volume-limited sample from the first data release of ZTF Hubble flow SNe Ia, we infer $H_0 = 76.94 \pm 6.4 \,\mathrm{km\ s^{-1}\ Mpc^{-1}}$, an 8.3% measurement. The error budget is dominated by the single object calibrating the SN Ia luminosity in this pilot study. However, the ZTF sample includes already five other SNe Ia within $\sim 20 \,\mathrm{Mpc}$ for which TRGB distances can be obtained with the Hubble Space Telescope. Finally, we present the prospects of building this distance ladder out to 80 Mpc with James Webb Space Telescope observations of more than 100 ZTF SNe Ia.

Key words: Observational cosmology – Hubble constant – Type Ia supernovae

1. Introduction

In recent years, a remarkable increase in accuracy obtained by a broad range of independent cosmological observations has provided compelling support for our current standard Λ cold dark matter model. This concordance cosmology successfully explains the measurements of fluctuations in the temperature and polarization of the cosmic microwave background (CMB) radiation (Planck Collaboration 2020) as well as observations of large-scale structure and matter fluctuations in the universe, e.g., baryon acoustic oscillations (Macaulay et al. 2019).

With improved accuracy of recent observations, some discrepancies have been noted. The prima facie most

Original content from this work may be used under the terms of the Creative Commons Attribution 4.0 licence. Any further distribution of this work must maintain attribution to the author(s) and the title of the work, journal citation and DOI.

significant tension is between the CMB inferred value of the Hubble constant (H_0) and the direct measurement of its local value (Riess et al. 2021). The local measurements are based on a calibration of the absolute luminosity of Type Ia supernovae (SNe Ia) using independent distances to host galaxies of nearby SNe Ia, known as the "cosmic distance ladder." This claimed tension, if confirmed, it could provide evidence for of new fundamental physics beyond the standard model of cosmology. It could, however, be a sign of unknown sources of systematic error. Currently, the local H_0 methods have slight differences in their values. The tip of the red giant branch (TRGB; Freedman 2021) and Cepheid (Riess et al. 2021) distance scales yield values of 69.8 ± 1.7 (however, see also Blakeslee et al. 2021, for example) and $73.04 \pm 1.04 \text{ km s}^{-1} \text{Mpc}^{-1}$, respectively. Understanding these differences is important to discern whether the tension is a sign of novel physics or a yetto-be-revealed systematic error. To date, only the TRGB and

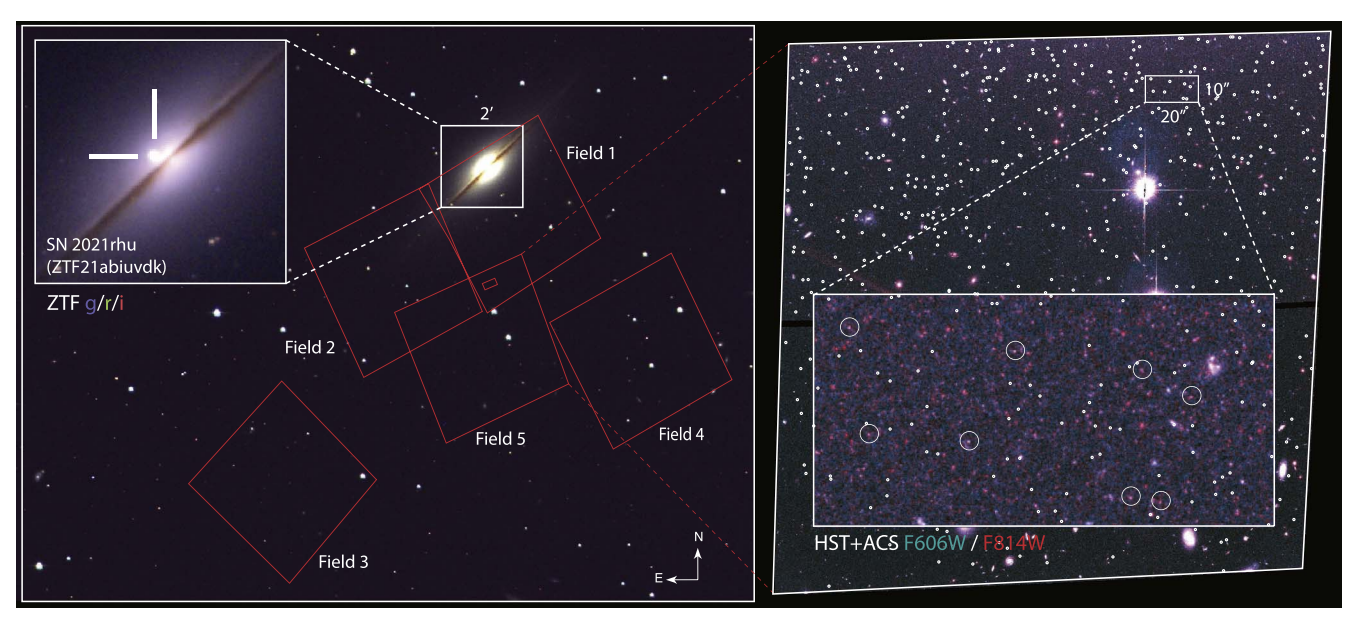


Figure 1. (Left) A combined color image of NGC 7814 from the ZTF gri data with Fields 1–5 from the HST ACS observations overplotted in red. The inset shows the central $2' \times 2'$ of NGC 7814 and the position of SN 2021rhu (upper left). (Right) HST ACS Field 5 (one of the three fields, along with Fields 3 and 4, used for the distance measurement) in the F606W and F814W filters. The inset panel (bottom left) is a $10'' \times 20''$ region showing individual stars near the tip of the red giant branch magnitude (marked as white circles).

Cepheid measurements have measured distances to 10 or more host galaxies of SNe Ia.

Circumventing the two largest known sources of systematic error is key to achieving the percent level precision in the local distance scale and resolving the Hubble tension. First, Cepheid variables strongly prefer young, star-forming environments. This has been shown to bias the inferred SN Ia luminosity, and hence H_0 (Rigault et al. 2020), though the size of this effect is currently debated (Jones et al. 2018). While the current Cepheid distance ladder, consisting of SNe Ia within a 40 Mpc volume in young, star-forming hosts (Riess et al. 2021), addresses this issue by evaluating H_0 from only the Hubble flow SNe Ia in low stellar mass hosts, it is important to measure H_0 using a volume-limited calibrator and Hubble flow sample of SNe Ia in all types of host galaxies, to quantify the environment dependent biases, given the profound cosmological implications of the Hubble tension. TRGB stars, unlike Cepheid variables, are found in both old and young environments; hence they can probe SNIa host galaxies of all morphological types in a given volume. The TRGB is a wellunderstood standard candle, arising from the core helium flash luminosity at the end phase of red giant branch (RGB) evolution for low-mass stars (Freedman et al. 2019; Freedman 2021; Jang et al. 2021). Furthermore, TRGB stars, found in the outskirts of galaxies, are less prone than Cepheids to biases from crowding, and are also comparatively less sensitive to reddening systematics, a potential contribution to the Cepheid H_0 measurements (e.g., Mortsell et al. 2022).

Second, the current sample of SNe Ia for H_0 measurements is derived from several (>20) different combinations of telescopes, instruments, and filters (e.g., Riess et al. 2021; Scolnic et al. 2021). Although there have been significant efforts to cross-calibrate the heterogeneous systems (Brout et al. 2021), there are irreducible uncertainties associated with the data where the filters, instruments, and even telescopes no longer exist. In light of these outstanding sources of error, it is

beneficial to have a volume-limited sample of calibrator and Hubble flow SNe Ia observed with the *same* instrument.

Addressing these issues, here we present a uniform distance ladder, with both calibrator and Hubble flow SNe Ia observed by the Zwicky Transient Facility (ZTF; Graham et al. 2019; Bellm et al. 2019), calibrated on the basis of the TRGB method. As both the calibrator and Hubble flow rungs of the distance ladder are observed with the same instrument, we only rely on a relative photometric calibration, which is a significantly simpler task than controlling the absolute calibration of an SN Ia sample. In this pilot study, we present ZTF calibrator SNe Ia within a nearby volume of luminosity distance, $D_L < 20$ Mpc and measure preliminary distances, where possible, for those SNe Ia using the TRGB. In the long term, we need a ZTF calibrator sample of \sim 100 SNe Ia to get to \sim 1% precision and accuracy on H_0 (assuming the current precision in the TRGB absolute magnitude calibration) to resolve the tension. With the James Webb Space Telescope (JWST) scheduled to start taking data in mid-2022, we can feasibly extend the calibrator rung to $D_L \sim 80\,$ Mpc. ZTF has already observed well-sampled light curves for more than 100 SNe Ia in this distance range. Therefore, within the $D_L \leq 80 \,\mathrm{Mpc}$ volume we will no longer be limited by the rate of SNe Ia in galaxies to obtain calibrator distances, currently a limiting factor for the largest calibrator sample (Riess et al. 2021).

2. Data and Methodology

We present the data for SNe Ia observed by ZTF in a $D_L < 20$ Mpc volume, for which there are sufficient observations to infer a distance from the TRGB method. While five SNe Ia have adequate light-curve sampling to get precise peak magnitude, shape, and color parameters from SNe Ia, only one of them, ZTF21abiuvdk (aka SN 2021rhu), has observations of the host galaxy to get an accurate distance.

SN 2021rhu exploded in NGC 7814 (see Figure 1, left inset), at $\alpha = 0.8143$, $\delta = 16.1457$ (J2000 coordinates), classified as

an SNIa on the Transient Name Server (SNIascore 2021; Munoz-Arancibia et al. 2021). We obtained photometry with a 1 day cadence for SN 2021rhu with ZTF, in the g, r, and i filters between -14.1 and +172.5 days. These observations begin on 2021-07-01.4 UTC. Hence, we obtained a densely sampled light curve with the ZTF observing system (Dekany et al. 2020), in multiple filters, i.e., the same system as the Hubble flow sample (as presented in Dhawan et al. 2022). The images were processed with the pipeline as detailed in Masci et al. (2019). The light curve, thus far, spans a large phase range from 2021-07-01.4 to 2021-11-11.11 (Figure 3 shows the range used in the fit). We have also obtained a well-sampled spectral time series, beginning with a classification spectrum with the SEDmachine (Blagorodnova et al. 2018; Rigault et al. 2019; Kim et al. 2022) on 2021 July 5. These are presented in detail in a companion paper (L. Harvey et al. 2022, in preparation). Figure 3 shows a maximum-light spectrum obtained with the SPectrograph for the Rapid Acquisition of Transients (Piascik et al. 2014) on the Liverpool Telescope (Steele et al. 2004).

SNe Ia distances are inferred from light-curve peak luminosity, shape, and color. The most widely used light-curve fitting algorithm, which we adopt for our analysis, is the Spectral Adaptive Lightcurve Template—2 (SALT2; Guy et al. 2007). This model treats the color entirely empirically, without distinguishing the intrinsic and extrinsic components. We use the most updated, published version of SALT2 (SALT2.4; see Guy et al. 2010; Betoule et al. 2014) as implemented in sncosmo v2.1.0¹⁸ (Barbary et al. 2016), identical to the lightcurve inference of the Hubble flow sample in Dhawan et al. (2022). In the fitting procedure, we correct the SN fluxes for extinction due to dust in the Milky Way (MW). Extinction values for the SN coordinates derived in Schlafly & Finkbeiner (2011) were applied, using the galactic reddening law proposed in Cardelli et al. (1989), with a total-to-selective absorption ratio, $R_V = 3.1$, the canonical MW value.

2.1. TRGB Distance Estimate

NGC 7814 was observed with the Advanced Camera for Surveys (ACS) on HST (see Figure 1) covering a total of seven fields as part of the GHOSTS survey (Radburn-Smith et al. 2011). Here, we reanalyze the data using a pipeline by the Carnegie-Chicago Hubble Program (Freedman et al. 2019), which implements its own point-spread function (PSF) fitting photometry based on DOLPHOT (Dolphin 2000) modeling synthetic PSFs with TinyTim (Krist et al. 2011).

The details of the pipeline can be found in Jang et al. (2021). We select Fields 3, 4, and 5 from the entire data set since Fields 1 and 2 are close to the disk of the galaxy and hence susceptible to high crowding and extinction biases, whereas Fields 6 and 7 are very sparse making it difficult to identify the TRGB. We perform artificial star tests, as a robustness test of the photometric pipeline, by injecting $\sim\!200,000$ stars into the calibrated, flat-fields and CTE-corrected individual exposure images and recover them using DOLPHOT. The artificial stars have a similar colors range to blue RGB stars in the shaded region of the CMD (see Figure 2). We populate stars within a brightness range of $25 < F814W \le 29$ mag. To mimic the observed spatial distribution and luminosity function (LF), we place more stars in the inner region of the galaxy.

The LF was binned with a width of 0.01 mag and smoothed with a Gaussian kernel of 0.1 mag (e.g., Figure 2). The edge detection is derived from the first derivative of the scale smoothed LF (see Hatt et al. 2017, for details). We perform a tip detection on each individual field and find the values to be consistent within errors and hence, take the average of the individual measurements with a conservative error for the TRGB. We find an MW extinction corrected tip at $F814W_{0,TRGB} = 26.81 \pm 0.06$ mag.¹⁹ Details of the tests, the impact of assumptions on the various components of the pipeline and consistency between the individual fields and with distances reported in the literature are presented in a companion paper (I.-S. Jang et al. 2022, in preparation). Inferring the distance to NGC 7814 from this tip measurement requires an absolute calibration of the TRGB magnitude. We use the most recent absolute calibration of the TRGB magnitude that is derived from multiple primary anchors, namely MW, the Large Magellanic Cloud (LMC). The Small Magellanic Cloud (SMC) and NGC 4258, from Freedman (2021), $M_{\rm F814W}^{\rm TRGB} = -4.049 \pm 0.038$ (see also, Li et al. 2022, for a new calibration from the MW) and we obtain a distance modulus of $\mu = 30.86 \pm 0.07$ mag. The individual sources of error in the final distance uncertainty are presented in Table 1. We note that there is debate in the literature regarding the value of this absolute magnitude, depending on the assumptions in the primary anchors. The TRGB magnitude can be calibrated using the parallax distances from the Gaia satellite early data release 3 (Gaia Collaboration et al. 2021) to MW globular clusters, e.g., ω Cen, detached eclipsing binary distances to the LMC and SMC (Pietrzyński et al. 2019; Graczyk et al. 2020) and the water maser distance to the nearby galaxy NGC 4258 (Reid et al. 2019). The difference assumptions/anchor combinations have led to a difference of up to ~ 0.1 mag in the inferred absolute magnitude. A summary of the various absolute calibrations in the literature are provided in Blakeslee et al. (2021), Freedman (2021).

We combine the calibrator data with the ZTF Data Release 1 (DR1) Hubble flow sample (Dhawan et al. 2022). TRGB stars are found in all types of SN Ia host galaxies and therefore, the TRGB-calibrated sample will be volume limited. To have a completely volume-limited distance ladder, i.e., both calibrator and Hubble flow rungs, in this study, we also only fit the volume-limited Hubble flow sample from ZTF DR1. However, we note that the ZTF Hubble flow SN Ia sample has been built with carefully controlled selection function via the Bright Transient Survey (e.g., Perley et al. 2020; Fremling et al. 2020). In future studies, this will be a unique advantage since we can use this to compute the selection effects for SNe Ia with redshifts up to $z \sim 0.1$, where the impact of peculiar velocity errors is significantly lower than for literature samples (see Dhawan et al. 2022, for details). For this study, since we are dominated in the uncertainty budget by having only a single calibrator, we conservatively take the sample to be complete to $z \le 0.06$. This selection cut reduces the Hubble flow sample from 200 to 98 SNe Ia.

3. Results

We fit the SALT2 light-curve model to the calibrator SN and get the peak luminosity, light-curve width, and color. We note

https://sncosmo.readthedocs.io/en/v2.1.x/

¹⁹ Data associated with Figure 2 can be found in https://github.com/hanlbomi/NGC7814-Field4.

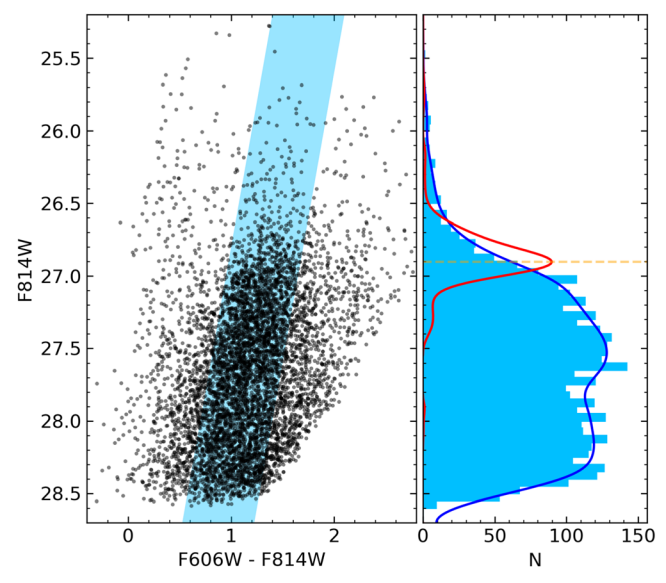


Figure 2. (Left) The color–magnitude diagram (CMD) for the RGB stars (black points) using the observed magnitudes in the F606W and F814W filters. The blue shaded area represents the color selection for the metal-poor RGB stars used in the TRGB determination. We show the CMD for Field 4 as an example of one of the fields that are used for the distance estimate in this work. The tip is detected using an edge detection method as detailed in Jang et al. (2021). (Right) The luminosity function (LF; blue histogram) for the RGB stars with the Gaussian smoothing using a 0.1 mag scale overplotted. The red curve shows the tip detection.

Table 1
The Statistical and Systematic Error Budget for Computing the TRGB, Shown for the Case of the Individual Field 4 As Used in Our Distance Determination

Effect	σ (mag)
Edge Detection	0.04
Photometry choice	0.02
Color selection	0.01
Smoothing selection	0.01
Empirical Aperture Correction	0.01
ACS Zero-Point	0.02
ACS EE Correction	0.02

that since SALT2 is not well defined at wavelengths redder than 7000 Å, we only fit the g and r filters (e.g., Jones et al. parameters has 2019). SN 2021rhu SALT2 $m_B = 12.22 \pm 0.033$, light-curve shape $x_1 = -2.074 \pm 0.025$, and color, $c = 0.054 \pm 0.028$. While the x_1 and c are within the range of typical cosmological cuts (e.g., $|x_1| < 3$, |c| < 0.3), it has a low x_1 value, which is also seen in peculiar, fast-declining SNe Ia. However, the light curves of SN 2021rhu show a clear shoulder in the r band and a second peak in the i band (Figure 3), characteristic of normal and transitional SNe Ia used for cosmology (Hsiao et al. 2015). We also compute the colorstretch parameter, s_{BV} , with the SNooPY method, since it is shown to be better at parameterizing the fast-declining SNe Ia (Burns et al. 2014). We find $s_{BV} = 0.72$ consistent with normal/transitional SNe Ia, appropriate to use for cosmology (Burns et al. 2018). It is also spectroscopically similar to transitional SNe Ia like SN 2011iv (Foley et al. 2012), which have been used for estimating H_0 (Freedman et al. 2019); thus this object is consistent with the cosmological sample of SNe Ia.

Here, we present the formalism for inferring H_0 . The absolute magnitude of SNe Ia, M_B , is given by

$$m_B^0 - \mu_{\text{host}} = M_B, \tag{1}$$

where m_B^0 is the *standardized* apparent peak magnitude of the SN Ia and μ_{host} is the distance modulus to the host galaxy based on the TRGB method. The Hubble flow SNe Ia measure the intercept of the magnitude–redshift relation, a_B . Ignoring higher order terms, the intercept is given by

$$a_{B} = \log cz + \log \left[1 + \frac{(1 - q_{0})z}{2} - \frac{(1 - q_{0} - 3q_{0}^{2} + j_{0})z^{2}}{6} \right] - 0.2m_{B}^{0}.$$
 (2)

We fix q_0 , j_0 , the deceleration and cosmic jerk parameters to the standard values of -0.55 and 1 respectively, since the low-z SN Ia sample alone cannot constrain them. We note that while cosmological studies with SNe Ia correct the redshifts for the Hubble flow sample accounting for peculiar motion due to local large-scale structure, this effect has been shown to be a subdominant source of error in measuring H_0 (Peterson et al. 2021), which is especially true here since only a single calibrator dominates the error budget. Additionally, we note that while this effect can be important when the calibrator sample is increased, as we have mentioned above, there will also be a simultaneous increase both in the size and the median redshift of the Hubble flow sample. m_B^0 is expressed in terms of the light-curve parameters and corrections as

$$m_R^0 = m_R + \alpha x_1 - \beta c - \delta_{\mu - \text{bias}}, \tag{3}$$

where α and β are the slopes of the width–luminosity and color–luminosity relations, respectively, and $\delta_{\mu-{\rm bias}}$ is the bias correction needed to account for selection effects and other sources of distance bias. Following the formalism of Brout et al. (2022), the canonical term for the host-galaxy "mass-step" correction is absorbed in the bias correction $\delta_{\mu-{\rm bias}}$ (see also Brout & Scolnic 2021). Since both the calibrator described by Equation (1) and the Hubble flow SNe Ia described by Equation (2) are constructed to be volume limited, such that they both have the *same* mass-step correction, the $\delta_{\mu-{\rm bias}}$ term will cancel out.

The error for each SN includes fit uncertainty from the SALT2 covariance matrix ($\sigma_{\rm fit}$), the peculiar velocity error ($\sigma_{\rm pec}$) and $\sigma_{\rm int}$:

$$\sigma_{\rm m}^2 = \sigma_{\rm fit}^2 + \sigma_{\rm pec}^2 + \sigma_{\rm int}^2. \tag{4}$$

For $\sigma_{\rm pec}$ we derive the magnitude error from a velocity error of 300 km s⁻¹ (Carrick et al. 2015). We use PyMultiNest (Buchner et al. 2014), a python wrapper for MultiNest (Feroz et al. 2009), to derive the posterior distribution on the parameters. With the current calibrator, we find, $H_0 = 76.94 \pm 6.4 \, {\rm km \, s^{-1} \, Mpc^{-1}}$. We also fit for H_0 using the entire Hubble flow DR1 sample and find $H_0 = 77.60 \pm 6.0 \, {\rm km \, s^{-1} \, Mpc^{-1}}$, a small difference of $0.66 \, {\rm km \, s^{-1} \, Mpc^{-1}}$. This uncertainty is not significantly smaller when using the entire gold sample for ZTF DR1 compared to the volume-limited one. This is because the main

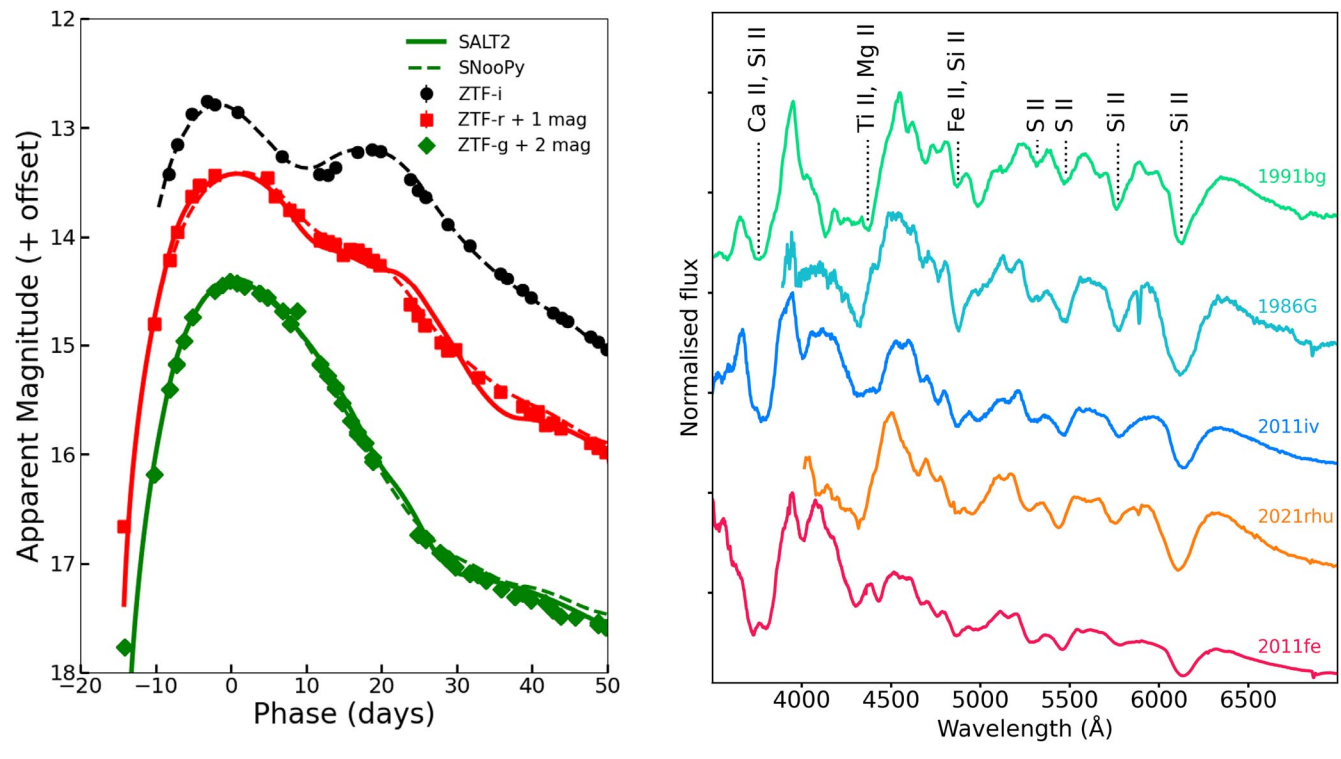


Figure 3. (Left) Light curve of SN 2021rhu in the g (green diamonds), r (red squares), and i (black circles) filters along with the SALT2 model fit to the g and r filters overplotted (solid) and the SNooPy model fit to the g, r, and i filters (dashed). The plot has truncated this the phase at which the SALT2 model is defined. (Right) A maximum-light spectrum of SN 2021rhu (orange), in comparison with the peculiar, subluminous SN 1991bg (green; Filippenko et al. 1992), transitional SN 1986G (cyan; Cristiani et al. 1992) and SN 2011iv (blue; Foley et al. 2012), the latter has been used as a calibrator object and the normal SN 2011fe (red; Parrent et al. 2012). The most common spectral features of intermediate mass and iron group elements of SNe Ia at maximum light are shown as dotted lines. We find that the near maximum-light spectrum of SN 2021rhu is very similar to transitional SNe Ia (see also L. Harvey et al. 2022, in preparation)

source of uncertainty is from having on a single calibrator object.

We also infer the corrected peak magnitudes with SNooPy (Burns et al. 2014). While SNooPy uses a light-curve template, as opposed to a spectral template for SALT2, it is trained with a larger sample of transitional SNe Ia similar to SN 2021rhu; hence we compare H_0 values from both methods. We compute distances to both the Hubble flow SNe Ia and SN 2021rhu with the EBV_model2. Using the same analysis method as for the SALT2 fitted distances, we infer an H_0 value of 77.58 \pm 6.1 km s⁻¹ Mpc⁻¹, a difference of 0.64 km s⁻¹ Mpc⁻¹ from the value using SALT2. This difference is significantly smaller than the uncertainty on H_0 from either method. Moreover, since SNooPy has a well-sampled training set to build the i-band template, we also infer H_0 from the g, r, and i filter combination and find a value of 76.17 \pm 6.0 km s⁻¹ Mpc⁻¹, a difference of 0.77 km s⁻¹ Mpc⁻¹ from the fiducial case.

4. Discussion and Conclusion

We present an estimate of H_0 from a uniform distance ladder using the same survey for the calibrator sample as a homogeneous, untargeted Hubble flow sample. We use a TRGB distance to a nearby host galaxy of an SN Ia with high-cadence data in the ZTF g, r, and i filters. The current uncertainty is not sufficient to weigh in on the Hubble tension. We note that even a factor of 2 reduction in the Hubble flow sample by imposing the volume limit does not impact the uncertainty on H_0 ; the error currently is driven by having only a single ZTF SNe Ia with robust, independent distances.

However, this can be increased with HST observations for nearby host galaxies. In the $D_L < 20$ Mpc volume, one where we can achieve completeness relatively quickly, ZTF has observed five more spectroscopically normal SNe Ia with well-sampled light curves, a sample expected to increase by $\sim 1-2$ per year for the remainder of ZTF operations. These SNe are

- 1. ZTF19aacgslb (SN 2019np) in NGC 3254;
- 2. ZTF20abijfqq (SN 2020nlb) in NGC 4382 (M85);
- 3. ZTF20abrjmgi (SN 2020qxp) in NGC 5002;
- 4. ZTF21aaabvit (SN 2021J) in NGC 4414;
- 5. ZTF21aaqytjr (SN 2021hiz) in UGC 7513.

All the SNe Ia listed above have coverage in the g, r, and ifilters beginning from at least 2 weeks before maximum light and extending beyond +70 days. We note that even with this small volume sample, there are early-type host galaxies like NGC 4382, for which other methods like Cepheid variables are not viable to obtain distances. In this volume, the number of calibrator SNe Ia is limited by the rate of SNe Ia exploding in the universe. The ZTF calibrator sample within the 20 Mpc volume accumulated to date is, however, sufficient to measure H_0 to \sim 3% accuracy using only HST for TRGB observations. In our analyses, we only infer the SN Ia light-curve parameters using g and r filters since SALT2 is not optimal for redder wave bands. Recently, improved SNe Ia models, e.g., SALT3 (Kenworthy et al. 2021), and/or BayeSN (Thorp et al. 2021; Mandel et al. 2022) have been demonstrated to enable an accurate use of redder wave bands, e.g., the ZTF i band. In future work, we will implement these models trained with highcadence ZTF SN Ia data in the g, r, and i wave bands to measure SN Ia distances. It has been demonstrated that the

Table 2
The Contribution from Individual Terms in the Error Budget for Measure H_0 with the Current Uniform Distance Ladder and the Forecast with Expected Distances from JWST

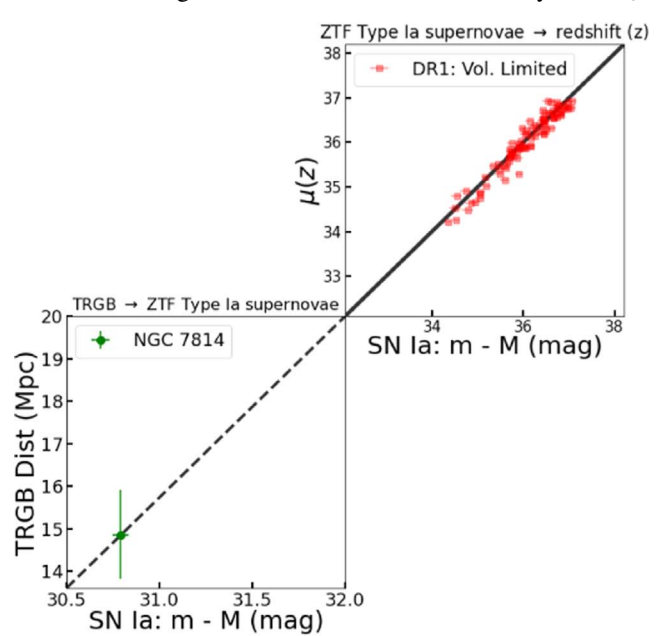
Quantity	Current Uncertainty (mag)	Expected Uncertainty (mag)
SN Ia intrinsic scatter	0.15	$0.1/\sqrt{100} = 0.01$
TRGB absolute calibration	0.038	0.023
TRGB in SN Ia hosts	0.05	$0.05/\sqrt{100} = 0.005$
Peculiar Velocity	0.02	0.01
Intercept of the Hubble diagram $(5a_B)$	0.013	0.004

improved SN Ia models can reduce the SN Ia intrinsic scatter to \lesssim 0.1 mag (e.g., see Mandel et al. 2022). We nominally expect the $\sigma_{\rm int}$ of a similar level when retraining the ZTF calibrator and Hubble flow samples with improved light-curve models (as assumed for Table 2). We note that our Hubble flow sample has only \sim 100 SNe Ia. This is due to two strict cuts. We apply both the restriction on a host spectroscopic redshift and the limit at the volume of $z \le 0.06$. The entire DR1 sample contains >750 SNe Ia (Dhawan et al. 2022), which is a significantly larger sample than the current Hubble flow rung in the literature. We have also shown here that H_0 inferred from the complete host spectroscopic redshift sample of SNe Ia, with a median z = 0.057, is consistent with our volume-limited subsample. The complete phase-I of ZTF operations has well-sampled light curves of ~ 3000 , of which ~ 650 are within the $z \leq 0.06$ volume. These have been discussed in Dhawan et al. (2022) and will be presented in future work as part of the ZTF second data release (DR2; M. Smith et al. 2022, in preparation). As discussed above, for the current work the Hubble flow sample is not the limiting factor in the final uncertainty on H_0 . However, going forwards the Hubble flow sample will be significantly augmented, both in terms of numbers and the maximum redshift to mitigate the impact peculiar velocity uncertainties (e.g., as demonstrated in Peterson et al. 2021). We summarize the forecast uncertainties in Table 2.

Future TRGB observations with the near-infrared camera (NIRCam) on JWST can extend the calibrator sample volume out to larger distances of up to 80 Mpc. In the volume $20 < D_L < 80$ Mpc, we have high-cadence light curves of 106 more SNe Ia already obtained (see Figure 4), expected to increase by the end of ZTF. Therefore, the complete sample of ZTF SNe Ia in a volume where JWST observations are feasible can increase the current calibrator sample by a factor of $\sim 2-3$. We emphasize that current SN Ia cosmology requires cross-calibrating several heterogeneous photometric systems (Brout et al. 2021). To get to percent level precision, it is an important cross-check to have observations of a large sample of SNe Ia on a single photometric system, which is the *same* for calibrator and Hubble flow SNe Ia.

While other concluded and/or ongoing SN Ia surveys have also observed SNe Ia in the distance range feasible for JWST, ZTF has two key advantages. First, the prospective calibrator sample of ZTF is \sim factor 2 larger in the same volume, since other surveys typically have \sim 50–60 SNe Ia in the specific distance range. This is important to increase the statistical power in the calibrator data set compared to the current calibrator sample. Second, there is a sizable Hubble flow sample of \sim 3000 SNe Ia, with a maximum redshift of z=0.1 (as discussed in Dhawan et al. 2022, and M. Smith et al. 2022, in preparation for the second data release) on the *same* photometric system as the calibrator sample, allowing us to reduce systematic errors both from cross-calibration uncertainties and dependence on the host-galaxy environment.

In addition to the improvements in the second and third rungs via the single system SN Ia sample proposed here, we



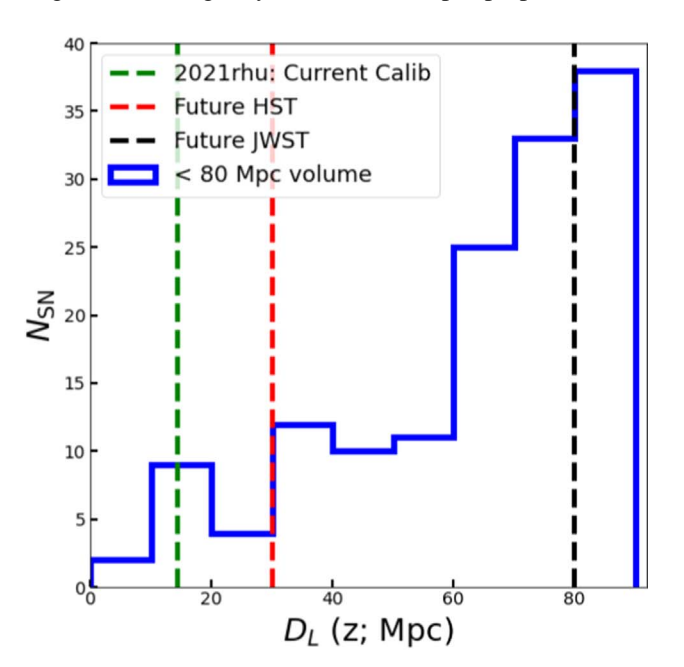


Figure 4. (Left): The current ZTF distance ladder with SN 2021rhu in NGC 7814 (green; the TRGB distance is plotted in linear scale instead of a distance modulus) and the volume-limited Hubble flow sample from ZTF DR1 (red). We emphasize that all SNe Ia in this distance ladder are observed with the same survey. (Right): Histogram of luminosity distances for nearby ($z \le 0.02$) ZTF SNe Ia with sufficient observations infer distances. Distances are computed from the redshift assuming standard cosmology from the Planck Collaboration et al. (2020) with $H_0 = 67.4$ km s⁻¹ Mpc⁻¹ and q_0 , j_0 of -0.55 and 1 respectively. Hence, they are only indicative. The distance for the current calibrator and the maximum distance feasible with HST and JWST are plotted as green, red, and black vertical dashed lines respectively. There is a total of 114 SNe Ia with high-quality light curves in this volume, providing a large sample to build a ZTF-only distance ladder.

would also expect improvements in the absolute calibration of the TRGB magnitude from a combination of multiple primary anchors. For the MW, an increase number of observations and a new full-scale astrometric solution in Gaia DR3 (and subsequently, DR4), compared to Early Data Release 3 (Lindegren et al. 2021) will decrease the random and systematic errors. Moreover, potential improvements in the extinction maps and primary distance calibration can also decrease the systematic errors in the calibration of the TRGB absolute magnitude from the Small and Large Magellanic Clouds compared to current measurements (Hoyt 2021). For NGC4258, with the maser distance, the current error budget in Jang et al. (2021) is conservative. Improvements in the zeropoint of the F814W filter and its EE correction as well as new observations of multiple halo fields of NGC4258 (Hoyt 2021) can appreciably reduce the systematic error. Assuming a 0.04 mag error in each of the primary calibrations, we expect a calibration of the TRGB magnitude to have a uncertainty of 0.023 mag (Table 2). More anchor galaxies, e.g., Sculptor (Tran et al. 2022) and Fornax (Oakes et al. 2022), can further reduce the uncertainty on the TRGB zero-point, especially with 1% parallaxes in the future (see Freedman 2021, for details). Future facilities can also increase the number of maser galaxies to calibrate the TRGB absolute magnitude by observing ideal candidates at significantly larger distances than the current, single calibrator galaxy, NGC 4258. In the case of the improved TRGB absolute magnitude calibration, this uniform distance ladder can measure H_0 at the $\sim 1.3\%$ level. However, the expected error with the current uncertainty on M_{TRGB} would be $\sim 1.8\%$, hence, sufficient for an independent TRGB estimate of H_0 , and arbitrating the Hubble tension. Hence, the increased statistical power and reduced systematic uncertainties from a single, untargeted survey make this an ideal approach to resolve the H_0 tension.

Based on observations obtained with the Samuel Oschin Telescope 48 inch and the 60 inch Telescope at the Palomar Observatory as part of the Zwicky Transient Facility project. Z. T.F. is supported by the National Science Foundation under grant No. AST-2034437 and a collaboration including Caltech, IPAC, the Weizmann Institute for Science, the Oskar Klein Center at Stockholm University, the University of Maryland, Deutsches Elektronen-Synchrotron and Humboldt University, the TANGO Consortium of Taiwan, the University of Wisconsin at Milwaukee, Trinity College Dublin, Lawrence Livermore National Laboratories, IN2P3, France, the University of Warwick, the University of Bochum, and Northwestern University. Operations are conducted by COO, IPAC, and UW. SEDMachine is based upon work supported by the National Science Foundation under grant No. 1106171. S.D. acknowledges support from the Marie Curie Individual Fellowship under grant ID 890695 and a Junior Research Fellowship at Lucy Cavendish College. A.G. acknowledges support from the Swedish Research Council under Dnr VR 2020-03444 and the Swedish National Space Board. This project has received funding from the European Research Council (ERC) under the European Union's Horizon 2020 research and innovation program (grant agreement No. 759194 -USNAC). Y.-L.K. acknowledges support by the Science and Technology Facilities Council [grant No. ST/V000713/1]. W. L.F. acknowledges support from program #13691 provided by NASA through a grant from the Space Telescope Science

Institute, which is operated by the Association of Universities for Research in Astronomy, Inc., under NASA contract NASA 5-26555. M.W.C acknowledges support from the National Science Foundation with grant numbers PHY-2010970 and OAC-2117997. This work was supported by the GROWTH Marshal project (Kasliwal et al. 2019) funded by the National Science Foundation under grant No. 1545949.

ORCID iDs

Suhail Dhawan https://orcid.org/0000-0002-2376-6979 Ariel Goobar https://orcid.org/0000-0002-4163-4996 Joel Johansson https://orcid.org/0000-0001-5975-290X Mickael Rigault https://orcid.org/0000-0002-8121-2560 Wendy L. Freedman https://orcid.org/0000-0003-3431-9135 Barry F. Madore https://orcid.org/0000-0002-1576-1676 Mathew Smith https://orcid.org/0000-0002-3321-1432 Jesper Sollerman https://orcid.org/0000-0003-1546-6615 Young-Lo Kim https://orcid.org/0000-0002-1031-0796 Igor Andreoni https://orcid.org/0000-0002-8977-1498 Eric C. Bellm https://orcid.org/0000-0001-8018-5348 Michael W. Coughlin https://orcid.org/0000-0002-8262-2924 Richard Dekany https://orcid.org/0000-0002-5884-7867 Shrinivas R. Kulkarni https://orcid.org/0000-0001-5390-8563 Russ R. Laher https://orcid.org/0000-0003-2451-5482 Michael S. Medford https://orcid.org/0000-0002-Guy Nir https://orcid.org/0000-0002-7501-5579 Reed Riddle https://orcid.org/0000-0002-0387-370X Ben Rusholme https://orcid.org/0000-0001-7648-4142

References

Barbary, K., Barclay, T., Biswas, R., et al. 2016, SNCosmo: Python library for supernova cosmology, Astrophysics Source Code Library, ascl:1611.017 Bellm, E. C., Kulkarni, S. R., Graham, M. J., et al. 2019, PASP, 131, 018002 Betoule, M., Kessler, R., Guy, J., et al. 2014, A&A, 568, A22 Blagorodnova, N., Neill, J. D., Walters, R., et al. 2018, PASP, 130, 035003 Blakeslee, J. P., Jensen, J. B., Ma, C.-P., Milne, P. A., & Greene, J. E. 2021, ApJ, 911, 65 Brout, D., & Scolnic, D. 2021, ApJ, 909, 26 Brout, D., Taylor, G., Scolnic, D., et al. 2021, arXiv:2112.03864 Brout, D., Scolnic, D., Popovic, B., et al. 2022, arXiv:2202.04077 Buchner, J., Georgakakis, A., Nandra, K., et al. 2014, A&A, 564, A125 Burns, C. R., Stritzinger, M., Phillips, M. M., et al. 2014, ApJ, 789, 32 Burns, C. R., Parent, E., Phillips, M. M., et al. 2018, ApJ, 869, 56 Cardelli, J. A., Clayton, G. C., & Mathis, J. S. 1989, ApJ, 345, 245 Carrick, J., Turnbull, S. J., Lavaux, G., & Hudson, M. J. 2015, MNRAS, Cristiani, S., Cappellaro, E., Turatto, M., et al. 1992, A&A, 259, 63 Dekany, R., Smith, R. M., Riddle, R., et al. 2020, PASP, 132, 038001 Dhawan, S., Goobar, A., Smith, M., et al. 2022, MNRAS, 510, 2228 Dolphin, A. E. 2000, PASP, 112, 1383 Feroz, F., Hobson, M. P., & Bridges, M. 2009, MNRAS, 398, 1601 Filippenko, A. V., Richmond, M. W., Branch, D., et al. 1992, AJ, 104, 1543 Foley, R. J., Kromer, M., Howie Marion, G., et al. 2012, ApJL, 753, L5 Freedman, W. L. 2021, ApJ, 919, 16 Freedman, W. L., Madore, B. F., Hatt, D., et al. 2019, ApJ, 882, 34 Fremling, C., Miller, A. A., Sharma, Y., et al. 2020, ApJ, 895, 32 Gaia Collaboration, Brown, A. G. A., Vallenari, A., et al. 2021, A&A, 649, A1 Graczyk, D., Pietrzyński, G., Thompson, I. B., et al. 2020, ApJ, 904, 13 Graham, M. J., Kulkarni, S. R., Bellm, E. C., et al. 2019, PASP, 131, 078001 Guy, J., Astier, P., Baumont, S., et al. 2007, A&A, 466, 11 Guy, J., Sullivan, M., Conley, A., et al. 2010, A&A, 523, A7 Hatt, D., Beaton, R. L., Freedman, W. L., et al. 2017, ApJ, 845, 146 Hoyt, T. J. 2021, arXiv:2106.13337

```
Hsiao, E. Y., Burns, C. R., Contreras, C., et al. 2015, A&A, 578, A9
Jang, I. S., Hoyt, T. J., Beaton, R. L., et al. 2021, ApJ, 906, 125
Jones, D. O., Riess, A. G., Scolnic, D. M., et al. 2018, ApJ, 867, 108
Jones, D. O., Scolnic, D. M., Foley, R. J., et al. 2019, ApJ, 881, 19
Kasliwal, M. M., Cannella, C., Bagdasaryan, A., et al. 2019, PASP, 131, 038003
Kenworthy, W. D., Jones, D. O., Dai, M., et al. 2021, ApJ, 923, 265
Kim, Y. L., Rigault, M., Neill, J. D., et al. 2022, PASP, 134, 024505
Krist, J. E., Hook, R. N., & Stoehr, F. 2011, Proc. SPIE, 8127, 81270J
Li, S., Casertano, S., & Riess, A. G. 2022, arXiv:2202.11110
Lindegren, L., Bastian, U., Biermann, M., et al. 2021, A&A, 649, A4
Macaulay, E., Nichol, R. C., Bacon, D., et al. 2019, MNRAS, 486, 2184
Mandel, K. S., Thorp, S., Narayan, G., Friedman, A. S., & Avelino, A. 2022,
MNRAS, 510, 3939
Masci, F. J., Laher, R. R., Rusholme, B., et al. 2019, PASP, 131, 018003
Mortsell, E., Goobar, A., Johansson, J., & Dhawan, S. 2022, ApJ, 933, 212
```

Munoz-Arancibia, A., Mourao, A., Forster, F., et al. 2021, Transient Name

Oakes, E. K., Hoyt, T. J., Freedman, W. L., et al. 2022, ApJ, 929, 116

Server Discovery Report, 2021-2265, 1

```
Parrent, J. T., Howell, D. A., Friesen, B., et al. 2012, ApJL, 752, L26
Perley, D. A., Fremling, C., Sollerman, J., et al. 2020, ApJ, 904, 35
Peterson, E. R., Kenworthy, W. D., Scolnic, D., et al. 2021, arXiv:2110.03487
Piascik, A. S., Steele, I. A., Bates, S. D., et al. 2014, Proc. SPIE, 9147, 91478H
Pietrzyński, G., Graczyk, D., Gallenne, A., et al. 2019, Natur, 567, 200
Planck Collaboration 2020, A&A, 641, A6
Planck Collaboration, Aghanim, N., Akrami, Y., et al. 2020, A&A, 641, A1
Radburn-Smith, D. J., de Jong, R. S., Seth, A. C., et al. 2011, ApJS, 195, 18
Reid, M. J., Pesce, D. W., & Riess, A. G. 2019, ApJL, 886, L27
Riess, A. G., Yuan, W., Macri, L. M., et al. 2022, ApJL, 934, L7
Rigault, M., Neill, J. D., Blagorodnova, N., et al. 2019, A&A, 627, A115
Rigault, M., Brinnel, V., Aldering, G., et al. 2020, A&A, 644, A176
Schlafly, E. F., & Finkbeiner, D. P. 2011, ApJ, 737, 103
Scolnic, D., Brout, D., Carr, A., et al. 2021, arXiv:2112.03863
SNIascore 2021, Transient Name Server Classification Report, 2021-2331, 1
Steele, I. A., Smith, R. J., Rees, P. C., et al. 2004, Proc. SPIE, 5489, 679
Thorp, S., Mandel, K. S., Jones, D. O., Ward, S. M., & Narayan, G. 2021,
      TRAS, 508, 4310
Tran, Q. H., Hoyt, T. J., Freedman, W. L., et al. 2022, arXiv:2205.08548
```